**NOTE • OPEN ACCESS**

# Rapid implementation of the repair-misrepair-fixation (RMF) model facilitating online adaption of radiosensitivity parameters in ion therapy

To cite this article: F Kamp *et al* 2017 *Phys. Med. Biol.* **62** N285

View the article online for updates and enhancements.

**Note**

# Rapid implementation of the repair-misrepair-fixation (RMF) model facilitating online adaption of radiosensitivity parameters in ion therapy

## F Kamp[1,2,3], D J Carlson[4] and J J Wilkens[1,2]

[1] Department of Radiation Oncology, Technical University of Munich, Klinikum rechts der Isar, Ismaninger Str. 22, 81675 München, Germany
[2] Physik-Department, Technical University of Munich, James-Frank-Str. 1, 85748 Garching, Germany
[3] Department of Radiation Oncology, Klinikum der Universität München, LMU Munich, Marchioninistr. 15, 81377 München, Germany
[4] Department of Therapeutic Radiology, Yale University School of Medicine, 333 Cedar St, New Haven, CT 06520-8040, United States of America

E-mail: florian.kamp@mytum.de and wilkens@tum.de

## Abstract

Introduction: Treatment planning for ion therapy must account for physical properties of the beam as well as differences in the relative biological effectiveness (RBE) of ions compared to photons. In this work, we present a fast RBE calculation approach, based on the decoupling of physical properties and the $\alpha_x/\beta_x$ ratio commonly used to describe the radiosensitivity of irradiated cells or organs.

Material and methods: In the framework of the mechanistic repair-misrepair-fixation (RMF) model, the biological modeling can be decoupled from the physical dose. This was implemented into a research treatment planning system for carbon ion therapy.

Results: The presented implementation of the RMF model is very fast, allowing online changes of $\alpha_x/\beta_x$. For example, a change of $\alpha_x/\beta_x$ including a complete biological modeling and a recalculation of RBE for $2.9 \cdot 10^5$ voxel takes 4 ms on a 4 CPU, 3.2 GHz workstation.

Discussion and conclusion: The derived decoupling within the RMF model allows fast changes in $\alpha_x/\beta_x$, facilitating online adaption by the user. This provides new options for radiation oncologists, facilitating online variations of the radiobiological input parameters during the treatment plan evaluation process as well as uncertainty and sensitivity analyses.

Keywords: repair-misrepair-fixation (RMF) model, relative biological effectiveness, RBE, ion therapy, treatment plan optimization

(Some figures may appear in colour only in the online journal)

## 1. Introduction

In carbon ion therapy, biological models are needed to predict the relative biological effectiveness (RBE) of carbon ions and lighter particles generated by nuclear fragmentation events. In the framework of the linear-quadratic (LQ) model (Kellerer and Rossi 1978) the cell survival is described by two radiosensitivity parameters: $\alpha$ (linear) and $\beta$ (quadratic). Biological models have been developed to estimate the particle radiosensitivity parameters ($\alpha_p$ and $\beta_p$) from the tissue specific, x-ray reference values ($\alpha_x$ and $\beta_x$). In the LQ model, RBE can be described by a function of $\alpha_x$, $\beta_x$, $\alpha_p$, $\beta_p$ and the physical dose $d$. Several biological models have been proposed and are currently used for the prediction of carbon ion RBE: different versions of the local effect model LEM1–LEM4 (Scholz *et al* 1997, Friedrich *et al* 2012, Grün *et al* 2012), the microdosimetric kinetic model (MKM) (Hawkins 1994, Kase *et al* 2008) and the repair-misrepair-fixation (RMF) model (Carlson *et al* 2008, Frese *et al* 2012, Kamp *et al* 2015). The LEM1 and the MKM are currently used in clinical practice. Typically, biological models, as well as their main input parameters, $\alpha_x$ and $\beta_x$, suffer from large uncertainties (Weyrather *et al* 1999, Carlson *et al* 2008), resulting in large confidence intervals for $\alpha_p$ and $\beta_p$.

At the moment these uncertainties have to be accounted for by the experience of radiation oncologists while three-dimensional evaluation of these uncertainties in treatment planning systems is very challenging. The current practice is a treatment plan evaluation based on model predictions for one specific set of $\alpha_x$ and $\beta_x$. The radiation oncologists have to include uncertainties in $\alpha_x$ and $\beta_x$ as well as in the biological modeling itself into the dose prescription and treatment plan evaluation without a possibility to quantify or simulate different biological modeling results. One of the main reasons is that the biological modeling process is computational intensive and takes long. The biological modeling process is generally slow as it has to be simulated over a broad range of ion types and energies, present in ion beams. This drawback is commonly overcome by precalculated and tabulated biological model output. Nevertheless, if e.g. $\alpha_x$ or $\beta_x$ should be changed after an optimization, the complete information needs to be generated again using another table. This does not allow frequent recalculations with different sets of radiosensitivity parameters, which would be needed for a biological uncertainty estimation of a carbon ion treatment plan.

In order to overcome this limitation in ion treatment plan evaluation, we present a decoupling approach within the framework of the repair-misrepair-fixation (RMF) model (Carlson *et al* 2008). The biological modeling is decoupled from the physical dose calculation and can be implemented very efficiently, facilitating online changes of x-ray radiosensitivity parameters in real time.

## 2. Material and methods

### 2.1. Treatment planning for carbon ion therapy

We implemented a multifield biological optimization for carbon ion therapy into an extension of the research treatment planning platform CERR (computational environment for radiation research) (Deasy *et al* 2003, Schell and Wilkens 2010, Kamp *et al* 2015, Brüningk *et al* 2015). CERR is a Matlab-based research treatment planning software. The presented workflow was implemented and evaluated using Matlab version 2013b. The ion therapy extension includes biological effect optimization, using a spot scanning beam delivery and a pencil beam dose algorithm. The calculations are based on tabulated Monte Carlo generated fragmentation spectra (Parodi *et al* 2012). These spectra contain data for all relevant ions types with atomic numbers $Z$ from 1 (protons) to 6 (carbon ions). For the calculations we implemented influence matrices which describe the influence of every spot $j$ on every voxel $i$ for dose $d_{ij}$, particle fluence and biological parameters (such that e.g. the dose in voxel $i$ becomes $d_i = \sum_j d_{ij} w_j$ for spot-weights $w_j$). The common, standard way to facilitate RBE calculations in a treatment planning system uses precalculated and tabulated biological modeling results ($\alpha_p$ and $\beta_p$) as function of water-equivalent depth for every available initial carbon ion energy. This means tables of $\alpha_p$ and $\beta_p$ values for every initial energy and every considered tissue type (characterized by $\alpha_x$ and $\beta_x$) are needed and stored with the tabulated depth dose curves. Depending on the chosen $\alpha_x$ and $\beta_x$ the right tables are used for the calculations, resulting in potentially inflexible situations (only precalculated $\alpha_x$–$\beta_x$ combinations can be used and once a combination is set it cannot be easily changed without redoing most of the calculation steps again).

### 2.2. The RMF model and the introduced decoupling approach

The biological modeling and the decoupling were achieved with the RMF model. The RMF model was introduced by Carlson *et al* (2008) and successfully implemented and validated for carbon ion, helium ion and proton treatment planning (Frese *et al* 2012, Kamp *et al* 2015, Mairani *et al* 2016). In the presented implementation, the mechanistic RMF model uses Monte Carlo damage simulation (MCDS) estimates of absolute double-strand break (DSB) yields (Semenenko and Stewart 2004, 2006, Hsiao and Stewart 2008, Stewart *et al* 2011). The link between DSB induction and cell death has been discussed in-depth previously by Carlson *et al* (2008), Stewart *et al* (2011, 2015) and references therein. Carlson *et al* (2008) and Frese *et al* (2012) showed how to determine particle radiosensitivity parameters $\alpha_p$ and $\beta_p$ from the reference radiosensitivity parameters $\alpha_x$ and $\beta_x$ and the MCDS output DSB induction $\Sigma$ and frequency-mean specific energy $\bar{z}_F$. The corresponding values for the reference radiation ($\Sigma_x$ and $\bar{z}_{F_x}$) are simulated based on the secondary electron spectra of a Co-60 source (Hsiao and Stewart 2008). MCDS 3.10A and the default cell nucleus diameter $d_{\text{tar}} = 5 \ \mu$m are used. Kamp *et al* (2015) combined the work of Frese *et al* (2012) with fragmentation spectra of carbon ion beams and implemented the RMF model in the standard, precalculated and tabulated way in a research treatment planning system, in order to show and discuss the influence of fragmentation spectra on RBE predictions by the RMF model.

　　The presented decoupling is based on the following equations (see also equations (3) and (4) of the work by Kamp *et al* (2015)). In order to differentiate between the different spots $j$ and voxel $i$, the dose averaged radiosensitivity values are written as $\alpha_{p,ij}$ and $\beta_{p,ij}$. The depth $z$ is included in the voxel $i$. $\Phi$ is the fluence spectrum of all fragmentation particles and $SP$ the stopping power, both are a function of the energy $E$ and the type (atomic number $Z$) of the ion.

$$\alpha_{p,ij} = \frac{\sum_Z \int_0^\infty \alpha_p\left(Z,E\right) \cdot \Phi_{ij}\left(Z,E\right) \cdot SP\left(Z,E\right) \mathrm{d}E}{\sum_Z \int_0^\infty \Phi_{ij}\left(Z,E\right) \cdot SP\left(Z,E\right) \mathrm{d}E} \tag{1}$$

$$= \alpha_{x,i} \frac{\sum_Z \int_0^\infty \left[\frac{\Sigma(Z,E)}{\Sigma_x}\right] \Phi_{ij}\left(Z,E\right) \cdot SP\left(Z,E\right) \mathrm{d}E}{\sum_Z \int_0^\infty \Phi_{ij}\left(Z,E\right) \cdot SP\left(Z,E\right) \mathrm{d}E}$$

$$+ \beta_{x,i} \frac{\sum_Z \int_0^\infty \left[2\frac{\Sigma^2(Z,E)}{\Sigma_x^2} \cdot \bar{z}_F\left(Z,E\right)\right] \Phi_{ij}\left(Z,E\right) \cdot SP\left(Z,E\right) \mathrm{d}E}{\sum_Z \int_0^\infty \Phi_{ij}\left(Z,E\right) \cdot SP\left(Z,E\right) \mathrm{d}E}$$

$$- \beta_{x,i} \frac{\sum_Z \int_0^\infty \left[2\frac{\Sigma(Z,E)}{\Sigma_x} \cdot \bar{z}_{F_x}\right] \Phi_{ij}\left(Z,E\right) \cdot SP\left(Z,E\right) \mathrm{d}E}{\sum_Z \int_0^\infty \Phi_{ij}\left(Z,E\right) \cdot SP\left(Z,E\right) \mathrm{d}E}$$

$$= \alpha_{x,i} \cdot c_{1,ij} + \beta_{x,i} \cdot c_{2,ij} \tag{2}$$

$$\sqrt{\beta_{p,ij}} = \frac{\sum_Z \int_0^\infty \sqrt{\beta_p\left(Z,E\right)} \cdot \Phi_{ij}\left(Z,E\right) \cdot SP\left(Z,E\right) \mathrm{d}E}{\sum_Z \int_0^\infty \Phi_{ij}\left(Z,E\right) \cdot SP\left(Z,E\right) \mathrm{d}E} \tag{3}$$

$$= \sqrt{\beta_{x,i}} \frac{\sum_Z \int_0^\infty \left[\frac{\Sigma(Z,E)}{\Sigma_x}\right] \Phi_{ij}\left(Z,E\right) \cdot SP\left(Z,E\right) \mathrm{d}E}{\sum_Z \int_0^\infty \Phi_{ij}\left(Z,E\right) \cdot SP\left(Z,E\right) \mathrm{d}E}$$

$$= \sqrt{\beta_{x,i}} \cdot c_{1,ij} \tag{4}$$

The RMF model with its decoupling parameters $c_1$ and $c_2$ (as introduced in equations (2) and (4)) has the very convenient property that $\alpha_{x,i}$ and $\beta_{x,i}$ can always be factored out. This means that in every voxel the biological radiosensitivity parameters can be separated from the physical beam properties ($d, \Phi, SP, \bar{z}_F, Z$) of the ions and their simulated DSB induction $\Sigma(Z,E)$. This decoupling can be done for any desired primary ion type, including their different fragment spectra and would equally work for Monte Carlo based dose calculations. $c_1$ can also be interpreted as the dose-weighted $\mathrm{RBE_{DSB}}$, defined as ratio of the DSB inductions: $\mathrm{RBE_{DSB}} = \Sigma\left(Z,E\right)/\Sigma_x$.

In equations (2) and (4) a very important relation becomes apparent. The needed values for $\alpha_p$ and $\beta_p$ are only dependent on $c_1$ and $c_2$ (besides the dependence on $\alpha_x$ and $\beta_x$ which are used to describe different tissue types). In the study by Kamp *et al* (2015) equations (1) and (3) were introduced, not mentioning and not exploiting the key property that $\alpha_p$ and $\sqrt{\beta_p}$ depend on the same two integrals (abbreviated with $c_1$ and $c_2$). A direct consequence is that for a given $\alpha_x$ and $\beta_x$, $\alpha_p$ and $\beta_p$ can be directly converted to $c_1$ and $c_2$ and vice versa. In the recent study, the $c_1$–$c_2$-formalism is introduced to fully exploit the simplicity which results from this property for RBE and RBE-weighted dose (RWD) calculations in ion therapy. This

relation is, too our knowledge, unique to the RMF model and a key feature for several shown and discussed implementations in the scope of this work.

The following equations give an overview of the implemented matrices as well as the physical and biological quantities that can be calculated in every voxel (i) for a given set of spot-weights $\omega_j$. The calculation of linear energy transfer (LET), $\alpha_{p,i}$ and $\beta_{p,i}$ is based on the work of Wilkens and Oelfke (2004, 2006).

$$d_i = \sum_j d_{ij} \cdot \omega_j \tag{5}$$

$$\text{LET}_i = \frac{1}{d_i} \sum_j \text{LET}_{ij} \cdot d_{ij} \cdot \omega_j \tag{6}$$

$$\alpha_{p,i} = \frac{1}{d_i} \sum_j \alpha_{p,ij} \cdot d_{ij} \cdot \omega_j \tag{7}$$

$$\sqrt{\beta_{p,i}} = \frac{1}{d_i} \sum_j \sqrt{\beta_{p,ij}} \cdot d_{ij} \cdot \omega_j \tag{8}$$

$$c_{1,i} = \frac{1}{d_i} \sum_j c_{1,ij} \cdot d_{ij} \cdot \omega_j \tag{9}$$

$$c_{2,i} = \frac{1}{d_i} \sum_j c_{2,ij} \cdot d_{ij} \cdot \omega_j \tag{10}$$

The dose-weighted calculation of $c_{1,i}$ and $c_{2,i}$ in the $ij$ formalism is very convenient, because it can be implemented in a treatment planning system exactly the same formalism as $d_i$, $\text{LET}_i$, $\alpha_{p,i}$ and $\sqrt{\beta_{p,i}}$. The same geometry, raytracing and water equivalent depths determination can be used for $c_1$ and $c_2$ as for e.g. the dose. This also means that the depth dependence along a pencil beam of $c_1$ and $c_2$ can also be precalculated and tabulated, identical to $d$, LET, $\alpha_p$ and $\sqrt{\beta_p}$ for different initial carbon ion energies. From the memory and time efficiency this means that using the introduced formalism, $\alpha_p$ and $\beta_p$ can be substituted by $c_1$ and $c_2$. Any desired $\alpha_x$ and $\beta_x$ can be multiplied later on. For other commonly used models, this is not possible because $\alpha_x$ and $\sqrt{\beta_x}$ cannot be always factored out. Equations (9)–(12) are derived in the Appendix. The here presented formalism is based on the property of the RMF model that $\alpha_{x,i}$ and $\beta_{x,i}$ can always be factored out and, hence, even be changed after an optimization without the need for much additional computation time. Using the RMF model, $\alpha_{p,i}$ and $\beta_{p,i}$ can be expressed similar to equations (2) and (4).

$$\alpha_{p,i} = \alpha_{x,i} \cdot c_{1,i} + \beta_{x,i} \cdot c_{2,i} \tag{11}$$

$$\beta_{p,i} = \beta_{x,i} \cdot (c_{1,i})^2 \tag{12}$$

Solving equations (11) and (12) for $c_{1,i}$ and $c_{2,i}$ shows how to determine these values from known $\alpha_{p,i}$ and $\beta_{p,i}$ distributions. A change of $\alpha_x$ and $\beta_x$ can be done very fast. It is based on $\alpha_{p,i}$ and $\beta_{p,i}$ only, without even the need to know the $ij$ matrices.

$$c_{1,i} = \sqrt{\frac{\beta_{p,i}}{\beta_{x,i}}} \tag{13}$$

$$c_{2,i} = \frac{\alpha_{p,i} - \alpha_{x,i}\sqrt{\frac{\beta_{p,i}}{\beta_{x,i}}}}{\beta_{x,i}} \tag{14}$$

These equations have a favorable consequence: it is actually not necessary to implement $c_{1,ij}$ and $c_{2,ij}$ explicitly. The standard $\alpha_{p,i}$ and $\sqrt{\beta_{p,i}}$ implementation can be used with an arbitrary value for $\alpha_{x,i}$ and $\beta_{x,i}$ and converted at any time to $c_{1,i}$ and $c_{2,i}$. This is useful to stay compatible with existing implementations of other biological models in a ion treatment planning system. Note that this calculation of $c_{1,i}$ and $c_{2,i}$ is independent of $d_i$, although $d_i$ is present in the dose-weighting in equations (9) and (10). Similar to equations (13) and (14), $c_{1,ij}$ and $c_{2,ij}$ can be calculated from $\alpha_{p,ij}$, $\beta_{p,ij}$, $\alpha_{x,i}$ and $\beta_{x,i}$ ($\alpha_{x,i}$ and $\beta_{x,i}$ are independent of the spot $j$).

The list of quantities that can be calculated in every voxel is completed by RBE and RWD. The dose $d_i$ is the dose per fraction. The general calculation of $\text{RBE}_{LQ,i}$ with $\alpha_{p,i}$ and $\beta_{p,i}$ being a function of $\alpha_{x,i}$, $\beta_{x,i}$ and parameters of the used biological model

$$\text{RBE}_{LQ,i}(\alpha_{x,i}, \beta_{x,i}, \alpha_{p,i}, \beta_{p,i}, d_i) = \frac{-\alpha_{x,i} + \sqrt{\alpha_{x,i}^2 + 4\beta_{x,i}(\alpha_{p,i}d_i + \beta_{p,i}d_i^2)}}{2\beta_{x,i}d_i} \tag{15}$$

can be rewritten using the decoupling of the RMF model by inserting equations (11) and (12) into equation (15). Hence $\text{RBE}_{RMF,i}$ can be calculated as

$$\text{RBE}_{RMF,i}\left(\frac{\alpha_{x,i}}{\beta_{x,i}}, c_{1,i}, c_{2,i}, d_i\right)$$
$$= \frac{1}{2d_i}\left(-\frac{\alpha_{x,i}}{\beta_{x,i}} + \sqrt{\left(\frac{\alpha_{x,i}}{\beta_{x,i}}\right)^2 + 4d_i\left(c_{1,i}\frac{\alpha_{x,i}}{\beta_{x,i}} + c_{2,i} + c_{1,i}^2 d_i\right)}\right). \tag{16}$$

In the framework of the RMF model, the calculation of $\text{RBE}_{RMF,i}$ is only dependent on $\alpha_{x,i}/\beta_{x,i}$ and not on $\alpha_{x,i}$ and $\beta_{x,i}$ individually. This was previously shown by Frese *et al* (2012) without the decoupling approach. The $\text{RWD}_i$ is calculated voxel-wise as

$$\text{RWD}_i = \text{RBE}_i \cdot d_i. \tag{17}$$

## 3. Results

We implemented the introduced $c_1$ and $c_2$ decoupling formalism and tested its performance. Figure 1 shows an example of a carbon ion treatment plan for an astrocytoma patient, previously treated with photons. The PTV was optimized on $\text{RWD} = 3$ Gy(RBE) using two fields as in Kamp *et al* (2015).

Panels A to D in figure 1 are the commonly shown optimization results $\text{RWD}_i$, $\text{RBE}_i$, $d_i$ and $\text{LET}_i$, respectively. The introduced decoupling parameters $c_{1,i}$ and $c_{2,i}$ are shown in panels E and F, together with $\alpha_{p,i}$ and $\beta_{p,i}$ in panels G and H, respectively. A spatially constant $\alpha_{x,i}/\beta_{x,i} = 2$ Gy ($\alpha_{x,i} = 0.1$ Gy$^{-1}$ and $\beta_{x,i} = 0.05$ Gy$^{-2}$ for all $i$) is used in this example treatment plan. These values are commonly used for sarcoma of the scull base (Schulz-Ertner *et al* 2007).
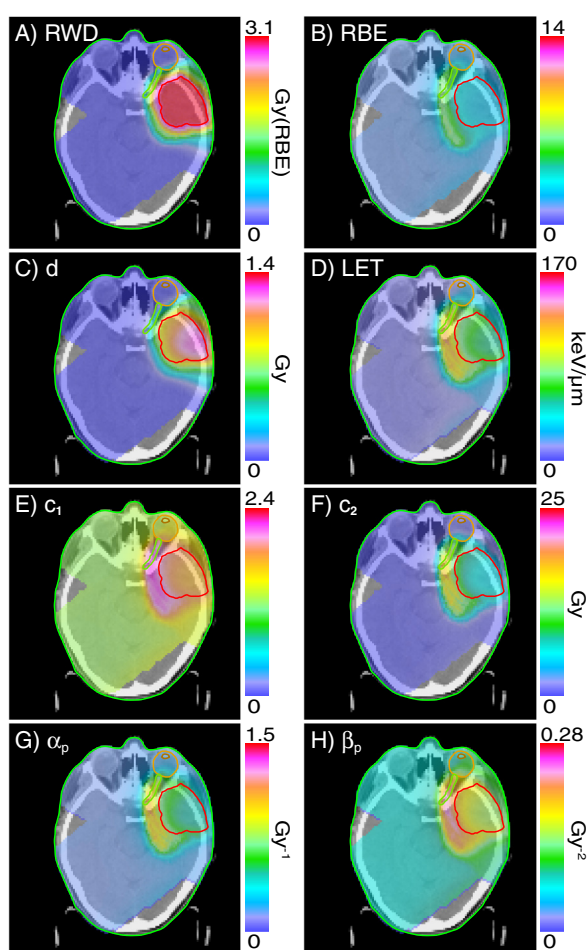
**Figure 1.** Axial CT slice of a treatment plan using the RMF model. The astrocytoma plan with two carbon ion fields was optimized on 3 Gy(RBE) with the ion therapy extension of the CERR treatment planning system using a spatially constant $\alpha_{x,i}/\beta_{x,i} = 2$ Gy ($\alpha_{x,i} = 0.1$ Gy$^{-1}$ and $\beta_{x,i} = 0.05$ Gy$^{-2}$). The PTV is shown in red, along with 3 organs at risk: left optic nerve (green), left eye (orange) and left lens (brown). The panels show (A) RWD$_i$, (B) RBE$_i$, (C) physical dose $d_i$ and the dose-weighted LET$_i$ in D. The two decoupling variables $c_{1,i}$ and $c_{2,i}$ are shown in panels E and F, along with the dose-weighted $\alpha_{p,i}$ and $\beta_{p,i}$ in panels G and H.

An evaluation possibility for online changes in the biological parameters is shown in figure 2. RBE-weighted dose-volume histograms (RWDVHs) are displayed for two representative structures. The initial RWDVH, optimized using $\alpha_{x,i}/\beta_{x,i} = 2$ Gy can be compared to the result of two modified $\alpha_{x,i}/\beta_{x,i}$. Note that the presented +20% change in $\alpha_x/\beta_x$ can be due to a 20% increase in $\alpha_x$ or a 20% decrease in $\beta_x$. RBE and hence RWD are only dependent on $\alpha_x/\beta_x$ and not $\alpha_x$ and $\beta_x$ independently (equation (16)).

Considering the whole patient, the values of the decoupling parameter $c_1$ range from 1.18 to 2.38 (mean 1.40, standard deviation 0.27, median 1.27), the values for $c_2$ from 0.37 Gy to 25 Gy (mean 2.64 Gy, standard deviation 3.71 Gy, median 0.75 Gy). The histograms and scatter plots in figure 3 show the distribution of resulting $c_1$ and $c_2$ values and their dependency on LET. The left part shows the values for all voxel inside the PTV structure (in total
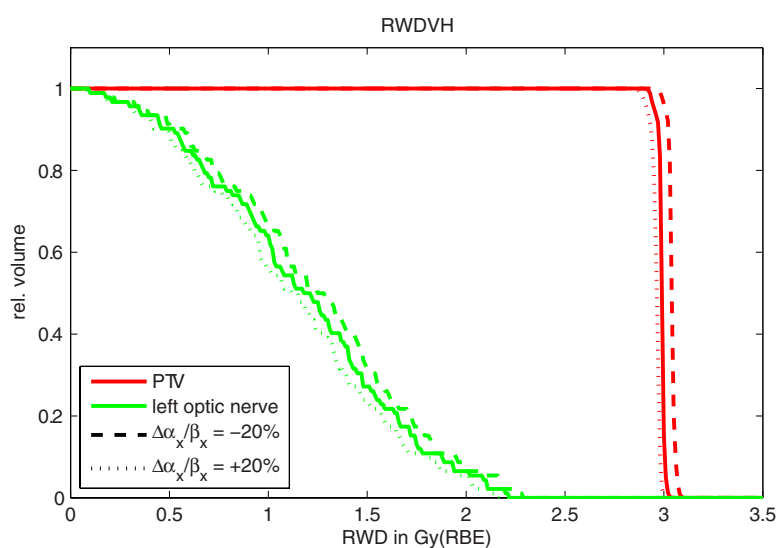
**Figure 2.** RBE-weighted dose volume histograms (RWDVHs) of the carbon ion treatment plan shown in figure 1. RWDVHs of two representative structures are shown: PTV and left optic nerve (organ at risk in the high LET region). The RWD distribution was initially optimized for a spatially constant $\alpha_{x,i}/\beta_{x,i} = 2$ Gy (continuous lines). The treatment plan was recalculated with a $\pm 20\%$ change in $\alpha_{x,i}/\beta_{x,i}$. The changes in the RWDVHs can be evaluated online using the presented decoupling formalism.

$3.5 \cdot 10^4$ voxel), the right part all voxel in the body structure without the PTV which receive a $\mathrm{RWD}_i > 0.1$ Gy(RBE) ($8.4 \cdot 10^4$ voxel). Both $c_1$ and $c_2$ are closely correlated to the LET distribution (Pearson correlation coefficients $\rho > 0.97$). The slopes of the linear regression lines for $c_1$ are 0.0087 $\mu$m keV$^{-1}$ and 0.0078 $\mu$m keV$^{-1}$ for PTV and 'body without PTV', respectively ($R^2 > 0.96$). The corresponding slopes for $c_2$ are 0.148 Gy $\mu$m keV$^{-1}$ and 0.156 Gy $\mu$m keV$^{-1}$ for PTV and 'body without PTV', respectively ($R^2 > 0.98$). Hence, the higher the LET value is the greater are $c_1$ and $c_2$. This trend can also be seen in the increase of $\alpha_p$ and $\beta_p$ distal to the PTV, which has been discussed comprehensively by Carlson *et al* (2008) and (Frese *et al* 2012). Figure 3 shows that the range of LET values and hence the range of $c_1$ and $c_2$ values inside the PTV is smaller than for the rest of the body. Considering the values in the PTV, LET ranges from 43 to 124 keV $\mu$m$^{-1}$ (mean 63 keV $\mu$m$^{-1}$, standard deviation 14.0 keV $\mu$m$^{-1}$, median 59 keV $\mu$m$^{-1}$), $c_1$ from 1.60 to 2.23 (mean 1.79, standard deviation 0.122, median 1.76) and $c_2$ from 3.86 to 16.7 Gy (mean 6.71 Gy, standard deviation 2.08 Gy, median 6.07 Gy). The corresponding values for the 'body without PTV' are LET from 16 to 160 keV $\mu$m$^{-1}$ (mean 63 keV $\mu$m$^{-1}$, standard deviation 31.8 keV $\mu$m$^{-1}$, median 58 keV $\mu$m$^{-1}$), $c_1$ from 1.28 to 2.38 (mean 1.74, standard deviation 0.254, median 1.72) and $c_2$ from 0.55 to 23.85 Gy (mean 7.24 Gy, standard deviation 0.500 Gy, median 6.36 Gy), respectively. The observed spread in $c_1$ and $c_2$ for constant LET (right panels of figure 3) originates from the fact that two different particle spectra can have the same dose-weighted LET value, but slightly different dose-weighted $c_1$ and $c_2$ and hence $\alpha_p$ and $\beta_p$.

After the optimization an online change of $\alpha_{x,i}/\beta_{x,i}$ can be done in 4 ms (for a stable timing in Matlab the mean value of 1000 changes was taken) if the value is changed throughout every voxel with $\mathrm{RWD}_i > 0$ Gy(RBE) ($2.9 \cdot 10^5$ voxel). A change in only a subset of the structures
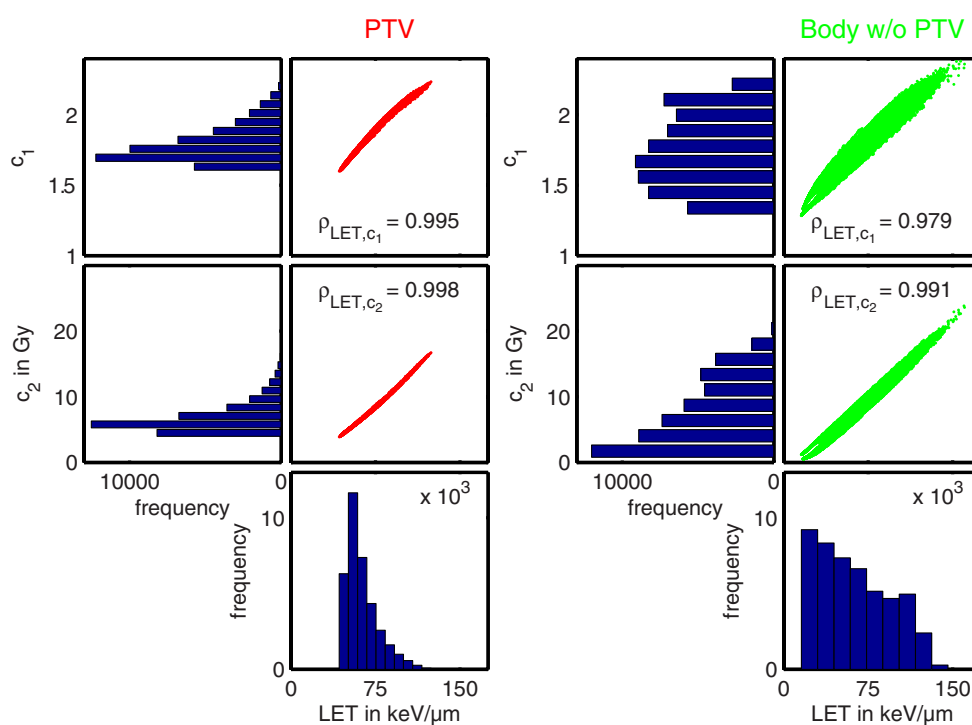
**Figure 3.** Distribution of $c_1$ and $c_2$ and their dependency on LET for the example treatment plan shown in figure 1. The plot is divided into values in the PTV (left, red, $3.5 \cdot 10^4$ voxel) and the 'body without PTV' (right, green, $8.4 \cdot 10^4$ voxel). Only values of voxel with $RWD_i > 0.1$ Gy(RBE) are considered in this figure. The corresponding Pearson correlation estimates $\rho$ are displayed in the panels.

is even faster, for example it took 1 ms (mean value of 1000 changes) for the PTV ($3.5 \cdot 10^4$ voxel, 270 cm$^3$). The calculations were performed on a 4 CPU, 3.2 GHz workstation. In the presented decoupling approach an (online) change of $\alpha_x/\beta_x$ represents a change in the biological dose response behavior, including a full biological modeling, whereas physical values as for example local particle spectra, LET and physical dose are kept constant.

## 4. Discussion

The presented implementation of the RMF model allows very fast changes of $\alpha_{x,i}$ and $\beta_{x,i}$ and hence online adaption of $\alpha_{x,i}/\beta_{x,i}$ and $RBE_{RMF,i}$. The changes can be done for every voxel independently. The shown decoupling is straight forward to implement in treatment planning systems, as $\alpha_{x,i}$, $\beta_{x,i}$, $\alpha_{p,i}$ and $\beta_{p,i}$ are commonly used. The decoupling, represented by $c_1$ and $c_2$ can be calculated before or after the generation of the $ij$ matrices or even after the optimization or after a forward calculation with given $\omega_j$. This can also be done for Monte Carlo based treatment planning, because the integration over the particle spectra (compare to equations (1) and (3)) are still independent of $\alpha_{x,i}$ and $\beta_{x,i}$.

The calculation time is very fast as it essentially consists of the time Matlab needed for two element-wise multiplications and a summation of vectors for $\alpha_{p,i} = \alpha_{x,i} \cdot c_{1,i} + \beta_{x,i} \cdot c_{2,i}$. For

the calculation of $\beta_{p,i} = \beta_{x,i} \cdot (c_{1,i})^2$, two element-wise multiplications are needed. The length of the vectors is the number of considered voxel. The time needed to do the same changes with the standard implementation (tabulated $\alpha_p$ and $\beta_p$) is not easily assessable, because the needed generation of new influence matrices and their subsequent handling is influenced by many other parameters. Common values for this lie in the range of several minutes.

The presented fast implementation of the RMF model is applicable for all currently discussed ion beams for radiotherapy. Accounting for the fragmentation spectra of the ion beams is straight forward and does not affect the calculation time per voxel for online $\alpha_{x,i}/\beta_{x,i}$ changes.

There are several possible applications for the presented biological modeling implementation. First of all this approach facilitates online adaption of the reference radiosensitivity parameters including a full biological modeling for RBE calculation. This can be used for online treatment plan evaluation, which can now, for example, include worst case scenarios for the biological response of tumor and normal tissue. The decoupling can be used for a systematical assessment of uncertainties in the RBE or RWD distributions, originating from confidence intervals of $\alpha_x$ and $\beta_x$. This facilitates comprehensive sensitivity analyses in three-dimensional, multifield geometries based on patient CT data (Böhlen *et al* 2012, Kamp *et al* 2014). In this context it has to be evaluated if it is sufficient to just change $\alpha_x$ and $\beta_x$, or if it is necessary to include further factors, like e.g. uncertainties in the biological modeling process. Fast biological modeling might in addition be useful for robust treatment plan optimization (Pflugfelder *et al* 2008, Unkelbach *et al* 2009, Bangert *et al* 2013) which aims to minimize the impact of uncertainties on a treatment plan.

## 5. Conclusion

The presented decoupling approach can be used for fast changes in the reference radiosensitivity parameters and is hence an important technical step towards online adaptation and evaluation of RBE-based treatment plans in ion therapy. This will help to estimate the impact of uncertainties in the biological modeling and the biological input parameters on treatment plans.

## Acknowledgments

## Appendix

In this appendix we briefly derive the calculation of $\alpha_{p,i}$ and $\beta_{p,i}$ in equations (11) and (12). The dose-weighted $c_{1,i}$ and $c_{2,i}$, calculated from their corresponding $ij$-matrices in equations (9) and (10) are introduced in the last line of the following equations. Note, that $\alpha_{x,i}$ and $\beta_{x,i}$ can have a different value in every voxel $i$ but do not depend on the spot $j$.

$$\alpha_{p,i} = \frac{1}{d_i} \sum_j \alpha_{p,ij} \cdot d_{ij} \cdot \omega_j$$

$$= \frac{1}{d_i} \sum_j \alpha_{x,i} \cdot c_{1,ij} \cdot d_{ij} \cdot \omega_j + \frac{1}{d_i} \sum_j \beta_{x,i} \cdot c_{2,ij} \cdot d_{ij} \cdot \omega_j$$

$$= \frac{\alpha_{x,i}}{d_i} \sum_j c_{1,ij} \cdot d_{ij} \cdot \omega_j + \frac{\beta_{x,i}}{d_i} \sum_j c_{2,ij} \cdot d_{ij} \cdot \omega_j$$

$$= \alpha_{x,i} \cdot c_{1,i} + \beta_{x,i} \cdot c_{2,i} \tag{A.1}$$

$$\sqrt{\beta_{p,i}} = \frac{1}{d_i} \sum_j \sqrt{\beta_{p,ij}} \cdot d_{ij} \cdot \omega_j$$

$$= \frac{1}{d_i} \sum_j \sqrt{\beta_{x,i}} \cdot c_{1,ij} \cdot d_{ij} \cdot \omega_j$$

$$= \frac{\sqrt{\beta_{x,i}}}{d_i} \sum_j c_{1,ij} \cdot d_{ij} \cdot \omega_j$$

$$= \sqrt{\beta_{x,i}} \cdot c_{1,i} \tag{A.2}$$

## References

Bangert M, Hennig P and Oelfke U 2013 Analytical probabilistic modeling for radiation therapy treatment planning *Phys. Med. Biol.* **58** 5401–19

Böhlen T T, Brons S, Dosanjh M, Ferrari A, Fossati P, Haberer T, Patera V and Mairani A 2012 Investigating the robustness of ion beam therapy treatment plans to uncertainties in biological treatment parameters *Phys. Med. Biol.* **57** 7983–8004

Brüningk S C, Kamp F and Wilkens J J 2015 EUD-based biological optimization for carbon ion therapy *Med. Phys.* **42** 6248

Carlson D J, Stewart R D, Semenenko V A and Sandison G A 2008 Combined use of Monte Carlo DNA damage simulations and deterministic repair models to examine putative mechanisms of cell killing *Radiat. Res.* **169** 447–59

Deasy J O, Blanco A I and Clark V H 2003 CERR: a computational environment for radiotherapy research *Med. Phys.* **30** 979–85

Frese M C, Yu V K, Stewart R D and Carlson D J 2012 A mechanism-based approach to predict the relative biological effectiveness of protons and carbon ions in radiation therapy *Int. J. Radiat. Oncol. Biol. Phys.* **83** 442–50

Friedrich T, Scholz U, Elsässer T, Durante M and Scholz M 2012 Calculation of the biological effects of ion beams based on the microscopic spatial damage distribution pattern *Int. J. Radiat. Biol.* **88** 103–7

Grün R, Friedrich T, Elsässer T, Krämer M, Zink K, Karger C P, Durante M, Engenhart-Cabillic R and Scholz M 2012 Impact of enhancements in the local effect model (LEM) on the predicted RBE-weighted target dose distribution in carbon ion therapy *Phys. Med. Biol.* **57** 7261–74

Hawkins R B 1994 A statistical theory of cell killing by radiation of varying linear energy transfer *Radiat. Res.* **140** 366–74

Hsiao Y and Stewart R D 2008 Monte Carlo simulation of DNA damage induction by x-rays and selected radioisotopes *Phys. Med. Biol.* **53** 233–44

Kamp F, Brüningk S C, Cabal G, Mairani A, Parodi K and Wilkens J J 2014 Variance-based sensitivity analysis of biological uncertainties in carbon ion therapy *Phys. Med.* **30** 583–7

Kamp F, Cabal G, Mairani A, Parodi K, Wilkens J J and Carlson D J 2015 Fast biological modeling for voxel-based heavy ion treatment planning using the mechanistic repair-misrepair-fixation model and nuclear fragment spectra *Int. J. Radiat. Oncol. Biol. Phys.* **93** 557–68

Kase Y, Kanai T, Matsufuji N, Furusawa Y, Elsässer T and Scholz M 2008 Biophysical calculation of cell survival probabilities using amorphous track structure models for heavy-ion irradiation *Phys. Med. Biol.* **53** 37–59

Kellerer A M and Rossi H H 1978 A generalized formulation of dual radiation action *Radiat. Res.* **75** 471–88

Mairani A *et al* 2016 Biologically optimized helium ion plans: calculation approach and its *in vitro* validation *Phys. Med. Biol.* **61** 4283–99

Parodi K, Mairani A, Brons S, Hasch B G, Sommerer F, Naumann J, Jäkel O, Haberer T and Debus J 2012 Monte Carlo simulations to support start-up and treatment planning of scanned proton and carbon ion therapy at a synchrotron-based facility *Phys. Med. Biol.* **57** 3759–84.

Pflugfelder D, Wilkens J J and Oelfke U 2008 Worst case optimization: a method to account for uncertainties in the optimization of intensity modulated proton therapy *Phys. Med. Biol.* **53** 1689–700

Schell S and Wilkens J J 2010 Advanced treatment planning methods for efficient radiation therapy with laser accelerated proton and ion beams *Med. Phys.* **37** 5330–40

Scholz M, Kellerer A M, Kraft-Weyrather W and Kraft G 1997 Computation of cell survival in heavy ion beams for therapy *Radiat. Environ. Biophys.* **36** 59–66

Schulz-Ertner D, Karger C P, Feuerhake A, Nikoghosyan A, Combs S E, Jäkel O, Edler L, Scholz M and Debus J 2007 Effectiveness of carbon ion radiotherapy in the treatment of skull-base chordomas *Int. J. Radiat. Oncol. Biol. Phys.* **68** 449–57

Semenenko V A and Stewart R D 2004 A fast Monte Carlo algorithm to simulate the spectrum of DNA damages formed by ionizing radiation *Radiat. Res.* **161** 451–7

Semenenko V A and Stewart R D 2006 Fast Monte Carlo simulation of DNA damage formed by electrons and light ions *Phys. Med. Biol.* **51** 1693–706

Stewart R D, Streitmatter S W, Argento D C, Kirkby C, Goorley J T, Moffitt G, Jevremovic T and Sandison G A 2015 Rapid MCNP simulation of DNA double strand break (DSB) relative biological effectiveness (RBE) for photons, neutrons, and light ions *Phys. Med. Biol.* **60** 8249–74

Stewart R D, Yu V K, Georgakilas A G, Koumenis C, Park J H and Carlson D J 2011 Effects of radiation quality and oxygen on clustered DNA lesions and cell death *Radiat. Res.* **176** 587–602

Unkelbach J, Bortfeld T, Martin B C and Soukup M 2009 Reducing the sensitivity of IMPT treatment plans to setup errors and range uncertainties via probabilistic treatment planning *Med. Phys.* **36** 149

Weyrather W K, Ritter S, Scholz M and Kraft G 1999 RBE for carbon track-segment irradiation in cell lines of differing repair capacity *Int. J. Radiat. Biol.* **75** 1357–64

Wilkens J J and Oelfke U 2004 Three-dimensional LET calculations for treatment planning of proton therapy *Z. Med. Phys.* **14** 41–6

Wilkens J J and Oelfke U 2006 Fast multifield optimization of the biological effect in ion therapy *Phys. Med. Biol.* **51** 3127–40